Use of Surface Water and Ocean Topography (SWOT) observations to support Land Use/Land Cover (LULC) change products: the case of the pacific coast of Ecuador

Valentine Sollier, Frédéric Frappart, Luc Bourrel, Bertrand Ygorra, Cassandra Normandin, Luis Huaraca, Thomasl P Couvreur, Edward Salameh, Nicolas Baghdadi, Jean-Pierre Wigneron

▶ **To cite this version:**

Valentine Sollier, Frédéric Frappart, Luc Bourrel, Bertrand Ygorra, Cassandra Normandin, et al.. Use of Surface Water and Ocean Topography (SWOT) observations to support Land Use/Land Cover (LULC) change products: the case of the pacific coast of Ecuador. Science of Remote Sensing, 2026, 13, pp.100410. ⟨10.1016/j.srs.2026.100410⟩. ⟨hal-05578828⟩

HAL Id: hal-05578828

https://hal.inrae.fr/hal-05578828v1

Submitted on 3 Apr 2026

HAL is a multi-disciplinary open access archive for the deposit and dissemination of scientific research documents, whether they are published or not. The documents may come from teaching and research institutions in France or abroad, or from public or private research centers.

L'archive ouverte pluridisciplinaire **HAL**, est destinée au dépôt et à la diffusion de documents scientifiques de niveau recherche, publiés ou non, émanant des établissements d'enseignement et de recherche français ou étrangers, des laboratoires publics ou privés.

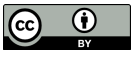

Distributed under a Creative Commons CC BY 4.0 - Attribution - International License

Science of Remote Sensing 13 (2026) 100410

Contents lists available at ScienceDirect

Science of Remote Sensing

journal homepage: www.sciencedirect.com/journal/science-of-remote-sensing

Use of Surface Water and Ocean Topography (SWOT) observations to support Land Use/Land Cover (LULC) change products: the case of the pacific coast of Ecuador

Valentine Sollier [a,b,*], Frédéric Frappart [a], Luc Bourrel [c], Bertrand Ygorra [a], Cassandra Normandin [a], Luis Huaraca [d], ThomasL.P. Couvreur [e], Edward Salameh [f], Nicolas Baghdadi [g], Jean-Pierre Wigneron [a]

[a] Institut National de Recherche Pour l'Agriculture, l'Alimentation et l'Environnement, Interactions Sol Plante Atmosphère, UMR1391, Bordeaux Science Agro, Villenave d'Ornon, France
[b] Institut national de recherche en sciences et technologies du numérique, Bordeaux Sud-Ouest, Talence, France
[c] Géosciences Environnement Toulouse, UMR 5563, Université de Toulouse, CNRS, IRD, OMP, CNES, Toulouse, France
[d] Subsecretaria de Calidad Ambiental, Ministerio de Ambiente Agua y Transición Ecológica, Quito, Ecuador
[e] DIADE, Université de Montpellier, Centre de coopération Internationale en Recherche Agronomique pour le Développement, Institut de recherche pour le développement, Montpellier, France
[f] Université Rouen Normandie, UNICAEN, CNRS, M2C UMR 6143, 76000, Rouen, France
[g] Institut National de Recherche Pour l'Agriculture, l'Alimentation et l'Environnement, UMR TETIS, Université de Montpellier, Montpellier, France

ARTICLE INFO

Keywords:
Surface water ocean topography
Land use/land cover
Pacific coast
Ecuador

ABSTRACT

Radar altimetry has been used to characterize land surfaces. However, the nadir configuration of the radar altimeter sensor and its coarse spatial resolution were limiting factor. The Surface Water and Ocean Topography (SWOT) mission overcomes these limitations through its Ka-band Radar Interferometer (KaRIn), a synthetic aperture radar (SAR) system, providing high spatial resolution and accurate surface height measurements. Initially used for hydrology and oceanography, this study explores an innovative use of SWOT to analyse changes in Land Use/Land Cover (LULC). To do this, three study areas located on the Pacific Coast of Ecuador were considered. The area in the south (A) is characteristic of cultivated areas, while the area in the center (B) presents a landscape mosaic and the area in the north (C) hosts tropical rainforests. For each study area, the SWOT backscatter coefficient (sig0) was analysed for the year 2024 from the raster product at 100m spatial resolution. We calculated the number of occurrences and the sig0 average from the raster product over each pixel. The spatial patterns obtained from these two variables enabled us to assign a LULC class (city, water, road, crop, or no forest, depending on the study area) to each pixel, using a Support Vector Machine (SVM). The assigned LULC classes depend on the partial spatial coverage of the SWOT data, which does not allow representing all the LULC classes. The classification results were compared with the LULC map provided by the Ministry of the Environment using a confusion matrix and obtained an accuracy greater than 0.87 and an F1 score greater than 0.89 for the three study areas. In the forest area (C), the SWOT observations were also compared to two change detection products: RAdar for Detecting Deforestation (RADD) alerts and detections by the Cumulative Sum (CuSum) method. 39% of the SWOT observations were in areas identified as *forest* by these products but classified as *no forest* or *water* in our SWOT classification. By detecting small streams (areas A, B and C), roads (area A), the boundaries of agricultural plots and the state of cultivated land (area A) as well as recent forms of deforestation (zone C), SWOT was found to be a complementary source of information for LULC change products.

* Corresponding author. Institut National de Recherche Pour l'Agriculture, l'Alimentation et l'Environnement, Interactions Sol Plante Atmosphère, UMR1391, Bordeaux Science Agro, Villenave d'Ornon, France.
E-mail address: valentine.sollier@inrae.fr (V. Sollier).

https://doi.org/10.1016/j.srs.2026.100410
Received 29 January 2026; Received in revised form 3 March 2026; Accepted 11 March 2026
Available online 12 March 2026
2666-0172/© 2026 The Authors. Published by Elsevier B.V. This is an open access article under the CC BY license (http://creativecommons.org/licenses/by/4.0/).

1. Introduction

Changes in Land Use/Land Cover (LULC), mainly due to the expansion and intensification of agriculture at the cost of forest cover, represent a growing risk to the stability of the Earth system (Foley et al., 2005; IPBES, 2019; Laurance et al., 2014). Ecosystem services provided by forests, essential for climate regulation, carbon storage, biodiversity conservation, and soil protection (Daily, 1997; Krieger, 2001) are threatened by anthropogenic pressures (Barlow et al., 2016) and climatic disturbance (França et al., 2020). According to the FAO (2022), South America has the highest rate of deforestation between 2000 and 2018. On this continent, Ecuador is the country most affected by deforestation (Mosandl et al., 2008; Armenteras et al., 2017), particularly the forests located on the Ecuadorian Pacific Slope and Coast (EPSC), which are considered a biodiversity hotspot (Myers, 1988). In this context, international initiatives such as the Reducing Emissions from Deforestation and Forest Degradation (REDD+) project (Matthews et al., 2014), also applied at national level as "Bosque para buen vivir" in Ecuador (Ministerio del Ambiente, 2017), demonstrate the importance of better understanding and characterizing the dynamics of LULC.

Remote sensing data is widely used to analyse LULC and their changes (Rogan and Chen, 2004; Sollier et al., 2025; Renaudineau et al., 2025). Multispectral images provided by optical sensors, such as MSI aboard Sentinel-2 (high spatial resolution of 10m) or MODIS aboard Terra (moderate spatial resolution of 500m), provide relevant information to distinguish between several types of land cover and are often used to form global databases such as Dynamic World (Brown et al., 2022) or land cover type product produced by NASA (Friedl and Sulla-Menashe, 2019). The set of optical images obtained from various missions such as AVHRR, MERIS, SPOT-VGT, PROBA-V and Sentinel-3 OLCI, used by ESA CCI (Copernicus Climate Change Service, 2019), provides an annual global land cover time series since 1992. On a global scale, Landsat images have also been widely used. Global Land Cover and Land Use Change (Potapov et al., 2022) use Landsat images coupled with observations from the GEDI LiDAR mission, which allows information on tree heights to be integrated. Other studies have focused on monitoring forest cover using Landsat images leading to the development of the Tropical Moist Forest (TMF) (Vancutsem et al., 2021) and Global Forest Change (Hansen et al., 2013) products. At the national level, the Ecuadorian Ministry of the Environment, Water and Ecological Transition (MAATE) (Ministerio del Ambiente, 2017) uses Landsat images to produce their national LULC maps. In regions where optical imaging is limited by cloud cover (Bossy et al., 2025), Synthetic Aperture Radar (SAR) sensors, such as Sentinel-1 and PALSAR-2, provide weather-independent information on surface structure and roughness and improve land cover mapping. The ESA WorldCover product (Zanaga et al., 2021) combines Sentinel-1 radar data and Sentinel-2 multispectral optical data to provide global land cover mapping at a spatial resolution of 10 m. JAXA provides annual global forest/no forest masks at 25 m of spatial resolution derived from L-band SAR images (Shimada et al., 2014). Less commonly, radar altimetry has also been used to characterize land surfaces using radar backscatter. For instance, several studies have demonstrated that radar altimetry can be exploited to characterize continental surfaces and their seasonal dynamics. Papa et al. (2003) have used dual-frequency (Ku and C) measurements from the Topex–Poseidon altimeter to produce global maps of radar backscatter coefficient (σ^0) and its seasonal variability, revealing contrasted signatures between deserts, floodplains, mountainous areas, and dense forests. Building on this work,(Frappart et al., 2015, 2021a,b) extended the analysis by investigating radar altimetry backscatter signatures using ERS-2, ENVISAT, Jason-1/2, and SARAL/AltiKa data covering the Ka, Ku, C, and S bands, confirming that backscatter varies systematically with surface type and season. Their results highlight low variability in arid and forested regions (<5 dB) and strong seasonal variability in savannas, rice fields, and floodplains (>20 dB), linked to soil moisture and flooding events. Together, these studies demonstrate that altimetric information combining the signal (σ^0) intensity, multi-frequency differences, and echo shape parameters provide a robust tool for surface type characterization, wetland detection, and monitoring of continental dynamics. However, all these radar altimetry missions have significant spatial limitations. The nadir configuration of the radar sensor limited measurements along the satellite groundtracks, and the coarse spatial resolution was a limiting factor in previous studies (Cretaux et al., 2023).

The Surface Water and Ocean Topography (SWOT) mission, launched in December 2022, allow overcoming the limitations of previous altimetry missions with a global continental cover and a repeat cycle of 21 days with a raster product at 100m spatial resolution (Fu et al., 2024; Biancamaria et al., 2016). SWOT's scientific advances are made possible using advanced technology. SWOT operates with a Ka-band Radar Interferometer (KaRIn), a synthetic aperture radar (SAR) system operating on near-nadir swaths, providing two swaths of 50 km each separated by a nadir gap of 20 km. (Fjortoft et al., 2014). The combination of the Ka band and this close nadir observation makes it possible to differentiate between water surfaces and surrounding land, even in complex topographical contexts or under dense vegetation cover (Fjortoft et al., 2014). Using AirSWOT, an airborne Ka-band radar simulator of the SWOT mission, Fayne et al. (2024) used Ka-band backscatter signatures to assess the ability of the future SWOT instrument to distinguish water surfaces from other types of cover. Simulations carried out using the Ka-band Phenomenology Scattering model (KaPS) provide insight into the behaviour of backscatter across fifteen land cover classes, including open water, dry and wet soils, emergent vegetation, and coastal areas. The results show that open water has a signature that is clearly distinct from land surfaces, up to five times more discriminating than dry soil classes, but that some confusion remains, particularly with saturated soils and water-land transition zones. The study also highlights that the angle of incidence influences the separability of classes, with low angles allowing for better distinction of flooded surfaces. These initial results confirm that SWOT data could be used to characterize continental surfaces, map the extent of surface water and detect flooding, even in the presence of vegetation or complex conditions. Kica et al. (2025) have evaluated the ability of the SWOT mission to measure water surface elevation (WSE) in herbaceous wetlands in the Everglades in Florida. By comparing SWOT data with *in situ* observations, the results showed excellent agreement with a correlation greater than 0.99 and an average absolute error of approximately 6.7 cm. These results show that SWOT is accurate in complex vegetated environments, providing reliable water level measurements and paving the way for better characterization of terrestrial wetlands. Salameh et al. (2024) have also showed that SWOT backscattering can be used to discriminate between sand, mud and water, allowing to map the elevation of intertidal flats. These innovative terrestrial applications of SWOT data open the way to new perspectives for the characterization of continental surfaces. The most recent studies by Bazzi et al., (2026a,b) have highlighted SWOT's ability to track soil moisture dynamics and detect irrigation on fields.

Although SWOT was designed primarily for hydrology and oceanography, its advanced features provide opportunities to develop new applications on the land use. This research explores the innovative use of SWOT to analyse changes in LULC that could provide complementary information to existing LULC products.

2. Materials and methods

2.1. Study area

Ecuador (81.03°W–75.16°W, 1.48°N–5.04°S) is in northwestern South America. In Ecuador, there are three main regions: the Andes that separate the Pacific coast (*Costa*), to the west and the Amazonian plain (*Oriente*) to the east. Our study focuses on three areas of the Pacific coast. Three study areas were chosen according to a double gradient of climatic

and anthropogenic pressures, which extends from south to north. The first area, the southernmost, is in the Guayas basin. This area is largely anthropized with an agricultural landscape and a dry tropical climate. The second, between the Coastal Cordillera and the Andean foothills, extends around the Daule Peripa hydroelectric dam with a highly fragmented seasonal tropical forest and marked anthropic influence. The last area is mainly in the province of Esmeraldas. It is an area a slightly anthropized with a tropical rainforest (Fig. 1).

2.2. Datasets

2.2.1. SWOT gridded data

The dataset used in this study is the SWOT gridded data corresponding to Level 2 High-Resolution Raster product (L2_HR_Raster) (JPL and Revision, 2025). These data are available with a spatial resolution of 100m and a temporal resolution of 21 days. Among the available variables, we use in this study the backscatter coefficient (noted Sig0) as well as the associated quality layer (*sig0_qual*). The values of the quality layers are 0, 1, 2 and 3 which indicate good, suspect, degraded and bad measurement, respectively. In this study, we analysed the data available for the year 2024. For area A, four tiles from the product SWOT L2 HR Raster were used: 313_075F, 313_076F, 466_079F and 466_080F. Area B is covered by three tiles: 035_077F, 188_078F and 466_078F, while area C consists of four tiles: 313_078F, 313_079F, 466_076F and 466_077F. For each of the three study areas, these different tiles partially overlap. The raster product is derived from the Pixel Cloud by aggregation of observations. The Pixel Cloud product provides point-based, geolocated measurements of water surface elevation, radar backscatter and associated quality information, all derived from the SWOT Ka-band radar interferometer. The Pixel Cloud product being filtered in order to retain only observations considered valid and of good quality, some pixels of the raster product do not have SWOT observations. Initially designed for hydrological applications, the Pixel Cloud is indeed filtered to only retain pixels identified as corresponding to water surfaces and exhibiting good interferometric coherence. The initial mission objective and the different filters explain the partial continental coverage of SWOT products. Moreover, valid SWOT observations are not systematically acquired on the same pixels during the year, which introduces temporal variability in spatial coverage. Thus, the raster product does not provide continuous data in space and time. SWOT products are available from NASA and CNES at https://search.earthdata.nasa.gov/or https://hydroweb.next.theia-land.fr/respectively.

2.2.2. Ancillary datasets

The first product used to compare SWOT observation is the LULC maps produced by the Ecuadorian Ministry of Environment, Water and Ecological Transition (MAATE). These maps are available with a spatial resolution of 30m, and for eight years from 1990. The most recent map we used in this study is available for 2022. The MAATE 2022 map is derived from satellite images of the advanced space thermal emission and reflection radiometer (ASTER), and generated using ISODATA unsupervised automatic classification (Ministerio del Ambiente, 2017). The MAATE maps were used in our study as a reference because the produced maps were validated and corrected by field data. The accuracy

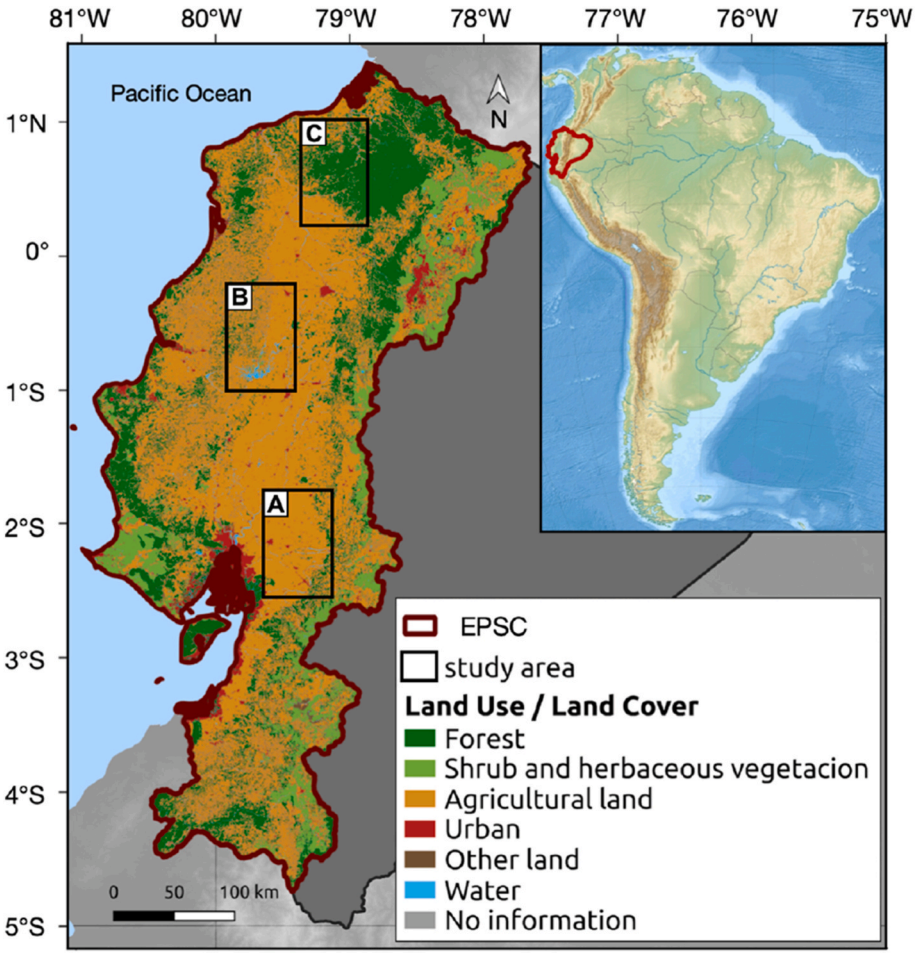

Fig. 1. Map of the Ecuadorian Pacific Slope and Coast (EPSC, red line) with the three selected study areas (black lines): area (A) in the south characteristic of cultivated areas and highly anthropized, area (B) in the middle extends around the Daule Peripa hydroelectric dam with seasonal tropical forest and marked anthropic influence and area (C) in the north a slightly anthropized with a tropical rainforest.

of the MAATE maps was estimated using the kappa index. A mean value of 0.7 was obtained for all maps. MAATE maps are available at: http://ide.ambiente.gob.ec/mapainteractivo.

The second product used to compare SWOT observations is RAdar for Detecting Deforestation (RADD) (Reiche et al., 2021). RADD alerts are derived from Sentinel-1 images with a spatial resolution of 10 m. Updates are made every 6 to 12 days. Alerts are generated from a single Sentinel-1 observation and then either confirmed or rejected over a period of up to 90 days based on the probability of forest disturbance. The RADD alert algorithm provides a mapping of new disturbances in primary rainforest from the primary forest mask defined by Turubanova et al. (2018), excluding historical losses and mangroves. The product has a minimum mapping unit (MMU) of 0.2 ha. Disturbances smaller than this threshold are not detected. RADD alerts were used until the end of the year 2024. RADD product is available free of charge from Google Earth Engine at: https://code.earthengine.google.com/6be36b448b13aeed914b4aff7d1510dd.

The third product used to evaluate the SWOT observations is the results obtained from the Cumulative Sum (CuSum) method of Ygorra et al. (2021). The CuSum method applied to Sentinel-1 images allows detecting trend breaks in the time series indicating a loss of forest cover. The algorithm calculates, for each pixel and each polarization (VV and VH), the cumulative sum of the deviations from the average of the backscattering signal. A significant variation in this sum indicates a change in the pixel. To strengthen the robustness of the detection, a bootstrap analysis must be computed to obtain a pixel-by-pixel confidence level. A spatial recombination between high and low confidence level results is then operated to combine the strengths of each confidence level. The minimum mapping unit is 0.03 ha. Sentinel-1 data has been analysed until the end of 2024.

Additional datasets were used to support the discussion and interpretation of the results. In particular, crop type maps provided by the Ecuadorian Ministry of Agriculture were employed. These vector datasets, available at a 1:25,000 scale, distinguish permanent crops: banana, oil palm, and sugarcane, available for the year 2022, as well as annual crops: rice, soya, and corn, available for the year 2024. Data on crop types from the Ministry of Agriculture are available at: http://geoportal.agricultura.gob.ec/.

The Global Land Use Land Cover map produced by Global Land Analysis and Discovery (GLAD) was also used. The most recent year available is 2020 and generated from Landsat images and GEDI data, allowing the integration of tree height information.

Finally, we used the high-resolution satellite images provided by Apple. These images are from third-party commercial suppliers such as Maxar, Airbus and Planet, and are composed of optical data corresponding to multisource mosaics. However, the proprietary provider does not publicly disclose the detailed metadata associated with these images, particularly the exact dates of image acquisition, which are therefore not accessible to the user. However, in the specific context of the north of the Pacific Coast of Ecuador (area C), optical data traditionally used as Sentinel-2 or Google Earth images are unusable because largely affected by cloud cover persisting throughout the year. In this case where no other recent and useable optical satellite imagery is available, Apple images provide access to visual information. These images thus offer a relevant support to conduct a qualitative visual analysis. The spatial resolution of these images is less than 1 m, allowing detailed identification of anthropogenic structures and vegetation cover, thus compensating for the limitations of conventional data sources.

2.3. Methodology

The general method is organized in three parts: 1) processing to filter SWOT observations, 2) classification of SWOT data using a machine learning model, support vector machine (SVM) (Vapnik, 1997) and 3) the comparison of SWOT observations classification with three products, MAATE LULC maps, RADD alerts and CuSum change detections.

2.3.1. SWOT data processing

The Sig0 SWOT data set for the year 2024 is filtered using the associated quality layer. The first applied filter removes pixels of poor quality. All pixels with a quality index of 2 and 3 which correspond to a degraded or bad quality measurement, are removed. The second filter is used to remove outliers and spatially isolated values. All groups of pixels made up of less than three pixels are removed. Furthermore, as Sig0 values are not normalised, the most extreme 0.10% of Sig0 values were discarded. At the end of this pre-processing, the processed data is used to calculate two variables. The first variable is the number of occurrences of each pixel during the year 2024 (layer: *number_occurrence*) by providing the observation frequency per pixel. This variable represents the spatial and temporal distribution of SWOT data. This variable highlights spatial patterns that are repeatedly observed over time. The raster product derived from the Pixel Cloud by aggregation implies that some pixels do not have SWOT observation. The Pixel Cloud product is filtered to retain only valid and good quality observations. Thus, the raster pixels do not systematically have data. Moreover, valid SWOT observations are not systematically acquired on the same pixels throughout the year. This specificity of SWOT data thus leads to a partial spatial coverage of SWOT observations, which the *number_occurrence* layer allows quantifying. The second variable calculated is the mean value sig0 (layer: *sig0_average*) representing the average intensity of the backscattered signal for the year 2024.

2.3.2. SWOT data classification

We used a Support Vector Machine (SVM) to perform a supervised LULC classification. The dataset for each of the three study areas (A, B and C) was created by selecting representative areas in each study area, corresponding to sub-areas of size 0.1 W × 0.1 H, where W and H denote the width and height of the study area respectively. The number of sub-areas used to create dataset depends on the study area because SWOT observations are not homogeneous across the entire territory and the number of SWOT observations are not identical depending on the study area considered. To reach approximately 10% of the known surface area each time, the number of areas is adapted to each region. For area A, we selected 5 zones, representing 9.71% of the study area. For area B, we selected 7 zones, accounting for 9.35% of the study area. For area C, 5 zones were selected, totalling 9.73% of the study area. Each of the areas that make up the dataset were manually classified using Google satellite images. The partial spatial coverage of the SWOT data does not allow all LULC classes to be represented. Areas A and B are characterized by extensive agricultural landscapes, where large-scale cultivated fields represent a dominant type of land cover, and four classes were defined: *city* (1), *water* (2), *road* (3), and *crop* (4). For the forest area (C), three classes were defined: *city* (1), *water* (2), *no forest* (3). Unlike areas A and B, area C is less anthropized, and most valid SWOT observations correspond to deforested or open areas, mainly located along communication routes. This motivated the use of a broader *no forest* class rather than a specific class of cropland.

The model was trained on 80% of the dataset, which was further split into 80% for training and 20% for validation. Given the limited number of labelled samples, a 80/20 split was preferred to maximize the amount of data available for training while still preserving a representative test set. The model was trained on a pair of data and labels denoted *(x;y)*. *x* represents the input data, which are the two rasters derived from the SWOT data obtained at the end of the previous step (*number_occurrence* and *sig0_average)*. *y* is the output labels; it represents the label corresponding to the land use type defined between 1 and 4, respectively for city, water, road, and crop. The model's input data is a vector of size 98. For each pixel to be classified, the 98-dimensions vector is obtained from the two input datasets: *number_occurrence* and *sig0_average*. For each input dataset, a 7 × 7 spatial neighbourhood around the central pixel to be classified is extracted, i.e. 49 values per dataset. The set of values from the two datasets is concatenated, resulting in a vector of 49 × 2 = 98. Preliminary experiments with different window sizes (3x3, 5x5, 7x7,

9x9 and 11x11) confirmed that the configuration with a 7x7 window offered the best compromise between classification accuracy and computational efficiency. The window size 7x7 is a good compromise between integrating sufficient spatial context and preserving fine-scale spatial patterns. At the end of training, the model was tested on the remaining 20% of the dataset. The labels predicted by the model were compared to the manual classification labels to evaluate the accuracy of the automatic classification.

Accuracy (1), F1-score (2) and Matthews Correlation Coefficient (MCC) (3) were calculated for each of the three areas. Each metric was calculated over 30 independent runs to estimate the average performance and variability of the model. Each run differs by the random initialization of model parameters and the random shuffling of training samples, allowing the quantification of inter-seed variability and the assessment of the robustness and stability of the model. The mean and standard deviation of these 30 runs were then reported. Accuracy is commonly used to evaluate the performance of a classification model and represents the ratio between the number of correctly predicted instances and the total number of instances in the dataset. F1 score and MCC provide additional information when classes are imbalanced (in our case, Cropland or No Forest class are overrepresented). F1 score is defined as the harmonic mean of precision (TP/(TP + FP)) and recall (TP/(TP + FN)). This indicator balances the importance of precision and recall and is preferable for datasets with class imbalance. However, F1 score may reach a limit in cases of extreme imbalance, as it does not take true negatives (TN) into account. The MCC allows all components of the confusion matrix (TP, TN, FP, FN) to be integrated, enabling it to measure an overall consistency regardless of class distribution. Consequently, the MCC can be more robust to class imbalance than the F1-score and provides a more reliable assessment in highly imbalanced multi-class scenarios (Chicco and Jurman, 2020).

$$\text{Accuracy} = \frac{TP + TN}{TP + TN + FP + FN} \tag{1}$$

$$F1 - score = \frac{2TP}{2TP + FP + FN} \tag{2}$$

$$MCC = \frac{TP \cdot TN - FP \cdot FN}{\sqrt{(TP + FP)(TP + FN)(TN + FP)(TN + FN)}} \tag{3}$$

The model was implemented in Python using the scikit-learn library, with a radial basis function (RBF) kernel with the default value of the γ (gamma) parameter of the scikit-learn RBF kernel allowing to consider non-linear separations between classes and a regularization parameter C = 0.9. Once trained, the model was applied to the entire study area to produce a classification map.

2.3.3. SWOT classification evaluation

For the three study areas, the classification maps obtained with SWOT data were evaluated by comparing them with the LULC maps of the MAATE using confusion matrices. The 2024 SWOT data was compared with the 2022 MAATE occupancy map, which is the most recent version currently available. The confusion matrices were computed considering three methodological constraints. The raster SWOT data, being derived from valid Pixel Cloud observations, do not cover all study areas, comparisons with MAATE data were limited to pixels for which observations were present. Moreover, as the MAATE does not distinguish between city class (1) and road class (3), these two categories were grouped under a single class, called 'urban'. Confusion matrices were performed only on comparable areas and classes. Thus, three classes were considered for comparison: urban, river, cropland (or no Forest for area C). For each of the three areas, the measures calculated from the confusion matrices are as follows: Accuracy (1), F1-score (2) and MCC (3).

Study area C is the only study area with a dense and continuous forest cover. As explained in the previous section, classified SWOT observations correspond to areas of deforestation. Thus, the SWOT observations will also be compared to RADD and CuSum data that provide information on changes in forest cover.

3. Results

3.1. Spatial pattern of Ka-band backscattering from SWOT

The spatial patterns obtained from the number of pixel occurrences (Fig. 2) and the Sig0 average over the year 2024 (Fig. 3) made it possible to characterize LULC. The two maps (Figs. 2 and 3) derived from SWOT data were used as input variables for a supervised classification model based on a Support Vector Machine (SVM). The average accuracy over 30 runs is 85% ± 0.35 for area A, 84% ± 0.52 for area B, and 89% ± 0.56 for area C. The average F1-score over 30 runs is 73% ± 0.98 for area A, 53% ± 0.87 for area B, and 64% ± 1.62 for area C. The average MCC over 30 runs is 64% ± 0.94 for area A, 70% ± 1.02 for area B, and 68% ± 1.82 for area C.

This model makes it possible to discriminate the main LULC classes. The automatic classifications obtained on the three study areas (Fig. 4) are presented according to the number of pixel occurrences to highlight the different spatial structures. The observation frequency and the average SWOT backscattering coefficient provide spatio-temporal information. The combined analysis of these two variables makes it possible to discriminate spatial structures and identify relevant patterns to characterize and obtain a classification of LULC from SWOT data (Fig. 4). In the two largely anthropized study areas, area A and area B, located respectively in the Guayas basin, and around the Daule Peripa hydroelectric dam, the training for classification was carried out on four LULC classes: city, road, water, and crop. However, unlike area A (Fig. 4a), in area B, the large predominance of other classes compared to road class did not allow this class to be included in the final classification (Fig. 4b). For area C, which extends from the Rio Cayapas to the Andean piedmont, the classification was carried out on three classes: city, water and No-Forest (Fig. 4c). The absence of SWOT observations is represented in white on all maps (Figs. 2–4).

The number of occurrences of each pixel in the SWOT data series provides information on the observation frequency of pixels. Each pixel indicates the number of times a valid observation was recorded (Fig. 2). In area A, the most heavily anthropized and characteristic of a dry climate (Fig. 2a), we observe frequent observations ranging up to 25 detections in 2024 across the entire study area. In area B (Fig. 2b), observations are focused on anthropized zones mainly in the region of the Daule Peripa hydroelectric dam. To the west of the study area, observations are less frequent in areas with fragmented seasonal forests. Conversely, in area C, which is less anthropized with a dense and continuous forest cover and a humid tropical climate (Fig. 2c), we observe less frequent observations that are localized in specific locations. Thus, we obtain spatial information from temporal information, with spatial patterns appearing depending on the type of activity present. Open and permanent water surfaces such as rivers have high occurrences. For instance, for areas A and B, the average number of occurrences in pixel corresponding to water surfaces is 17.8 ± 5.4 and 16.2 ± 6.4 observations respectively (Fig. 4a and b). For area C, the average value is slightly lower with an average number of occurrences of 12.5 ± 6.6 detections (Fig. 4c). These values reflect a strong occurrence of observations in water environments. Cities also have a high number of pixel occurrences, with an average of 14.2 ± 5.4 for area A and 12.1 ± 5.4 for area B and 13.3 ± 5.1 for area C. Conversely, agricultural areas present lower occurrences with average values of 4.2 ± 4.0, 2.7 ± 2.5, and 2.4 ± 2.0 for areas A, B and C respectively but also more heterogeneous, reflect less frequent and more variable observations (Fig. 4a and b). Thus, the number of pixel occurrences varies from the highest values in the north of area A, to the lowest in the south (Fig. 4a) through intermediate values in the center of area B (Fig. 4c). The roads detected by SWOT have intermediate average values, between 10.5 ± 4.4 and

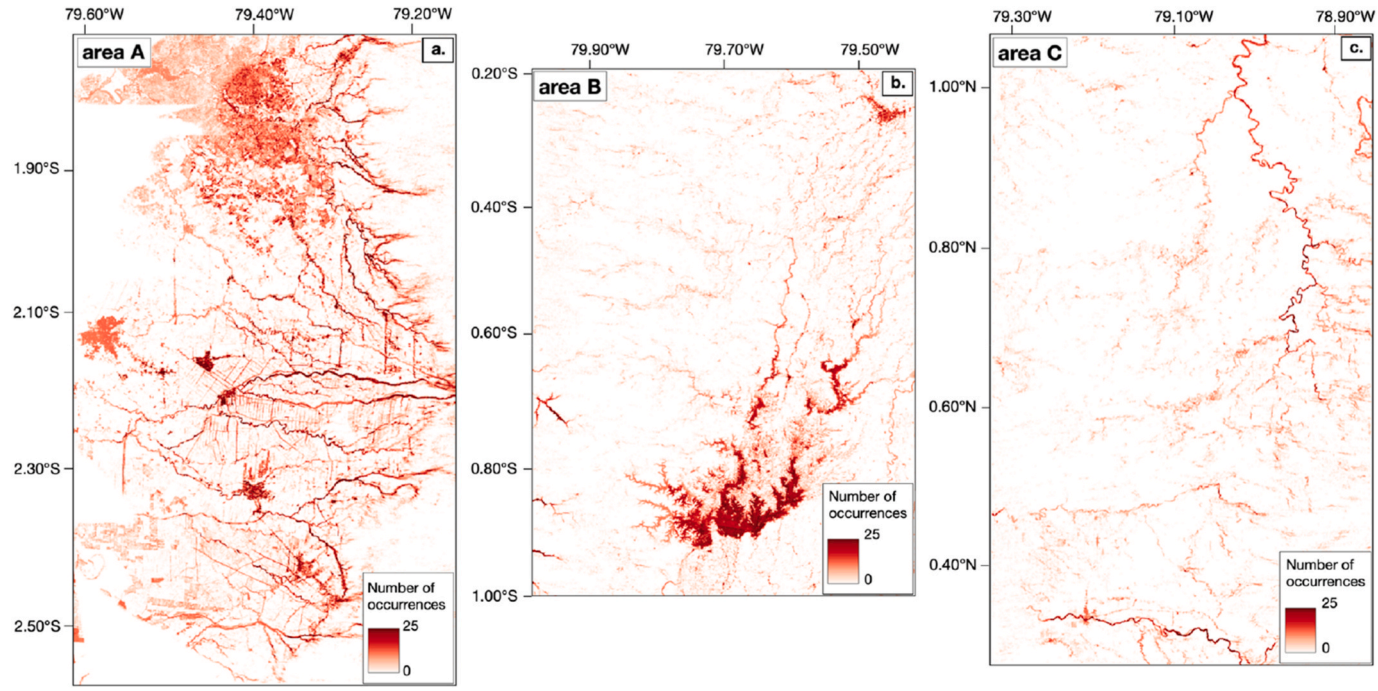

Fig. 2. Number of occurrences for each pixel, providing the observation frequency per pixel for the year 2024 for a) area A (cultivated area), b) area B (mosaic landscape) and c) area C (tropical forest).

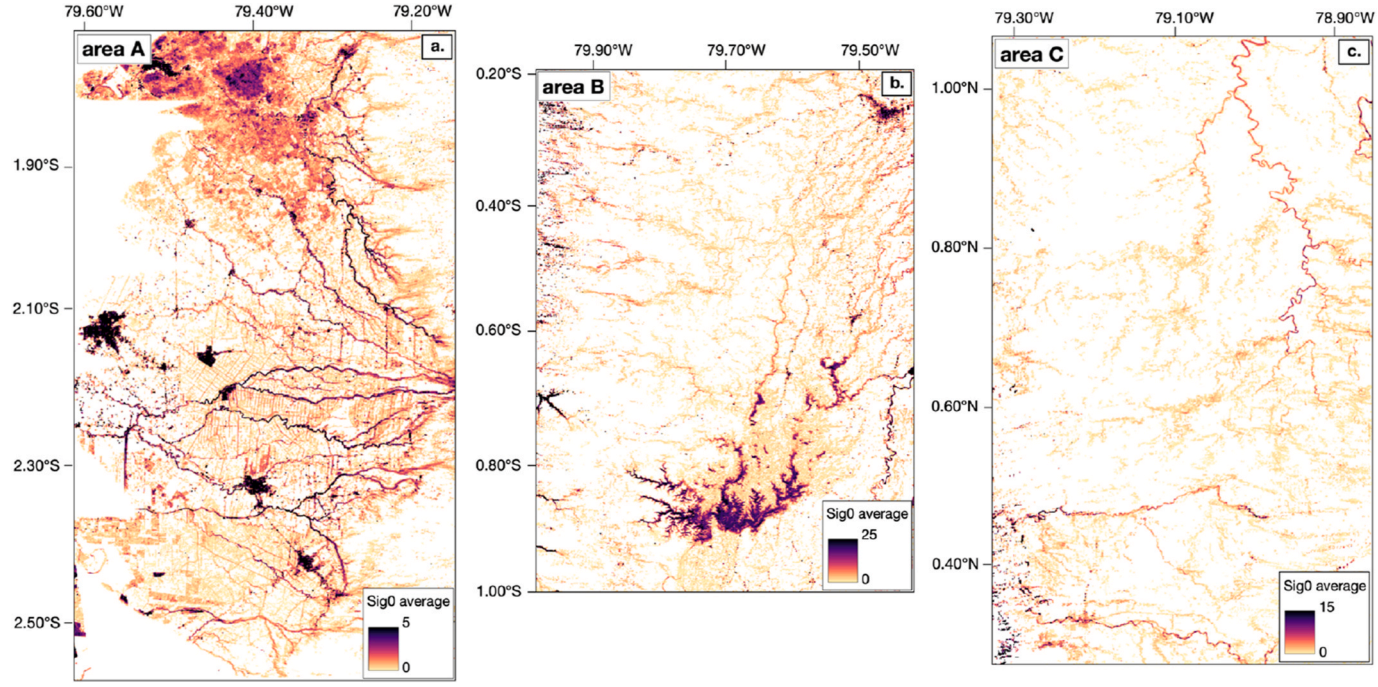

Fig. 3. Observed SWOT backscatter coefficient (Sig0 average) for the year 2024 for a) area A, b) area B and c) area C.

11.1 ± 3.3 for areas A and C. The classification obtained made it possible to highlight the boundaries of agricultural plots mainly in the center and south of study area A, southeast of the city of Naranjito (Fig. 4a). The classification based on observation frequency therefore provides a temporal indication, which allows distinguishing different patterns and highlighting spatial structures.

The average backscatter coefficient (sig0) calculated over the entire SWOT series in 2024 provides radiometric information that varies depending on the type of surface present. The backscattering coefficient is expressed in linear scale and not converted to decibels because each study area is analysed independently. In each study area, the use of linear scale values allows direct observation of spatial contrasts, which allow for the analysis of spatial structures and patterns conducted in this study. (Fig. 3). Thus, the low amplitude of the values of sig0 in area A is represented with a scale up to 5 (Fig. 3a) while the high values of sig0 in area B are represented with a scale up to 25 (Fig. 3b). Between the two, the area C presented a maximum value of 15 (Fig. 3c). However, for areas A and B, the cities have the highest backscattering coefficient of,

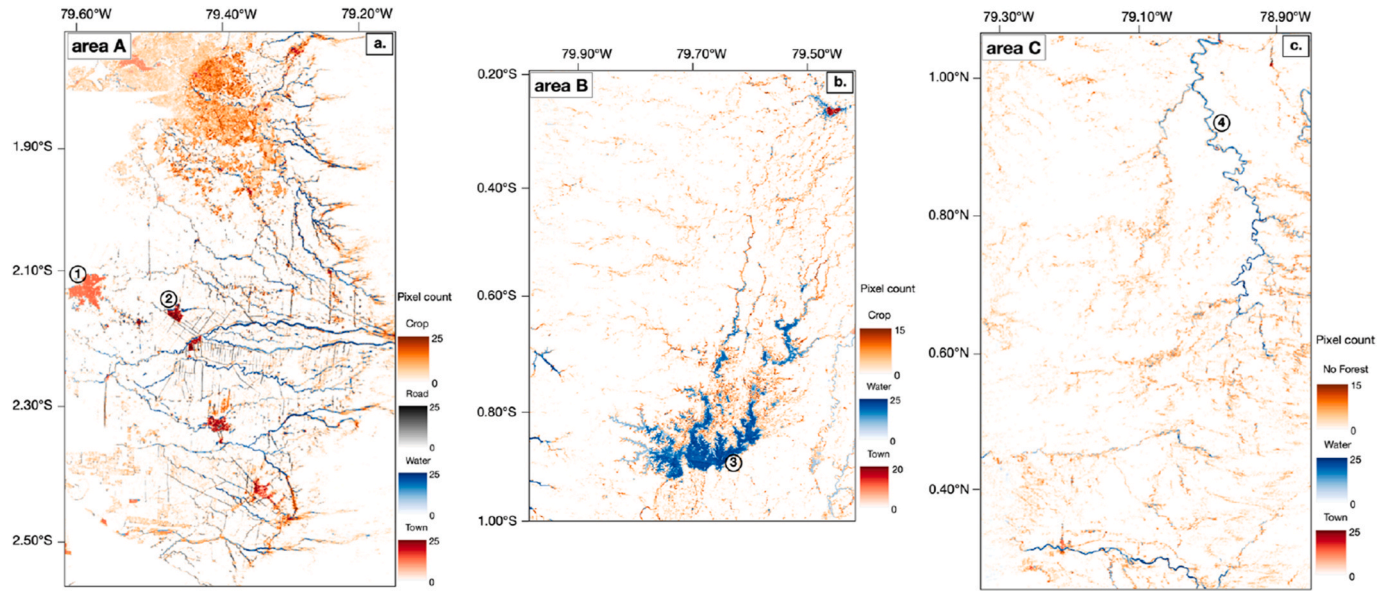

Fig. 4. Cover type classification based on SWOT data depending on *number of occurrences* obtained with an SVM over areas A, B and C. a) For area A, four classes: City, Water, Road and Cropland with the number 1 corresponding to the city of Milagro and the number 2 corresponding to the city of Naranjito, b) For area B, three classes: City, Water and Cropland with the number 3 corresponding to the Daule Peripa dam, and c) for area C, three classes: City, Water and No Forest with the number 4 corresponding to the Cayapas river's.

6.5 ± 4.2 and 29.5 ± 13.2 respectively, relative to the amplitude of the Sig0 values for each area. In these same two areas, the water zones also have a mean Sig0 that remains high with an average of 3.6 ± 2.5 for area A and 15.1 ± 16.3 for area B (Fig. 4a and b). Conversely, for area C, the highest average values correspond to open water areas with sig0 average of 6.6 ± 10.2, and the cities have a lower average with sig0 average of 5.4 ± 3.5 (Fig. 4c). The lowest mean values are associated with cultivated areas: 0.8 ± 0.9 for area A, 2.9 ± 7.4 for area B, and 0.9 ± 1.6 for area C. Nevertheless, the type of crop in presence can strongly influence the radar backscattering, which explains the significant spatial variation in the Sig0 values on cultivated areas (Fig. 4a). For area C, observations with low backscatter to the east of the study area correspond to areas classified as non-forest by SVM (Fig. 3c). Nevertheless, these SWOT observations are within the forest cover provided by the Ministry (Fig. 4c). It is likely that the linear structures crossing wooded areas to the east of the zone correspond to human activities detected by SWOT in the forest area. Other observations along the tributaries of the Cayapas River reflect forest dynamics in a wetland environment. The roads have intermediate average values between 1.6 ± 1.6 for area A and 4.9 ± 4.6 for area C. This radiometric parameter provides additional spatial information allowing the characterization of surfaces according to their backscatter.

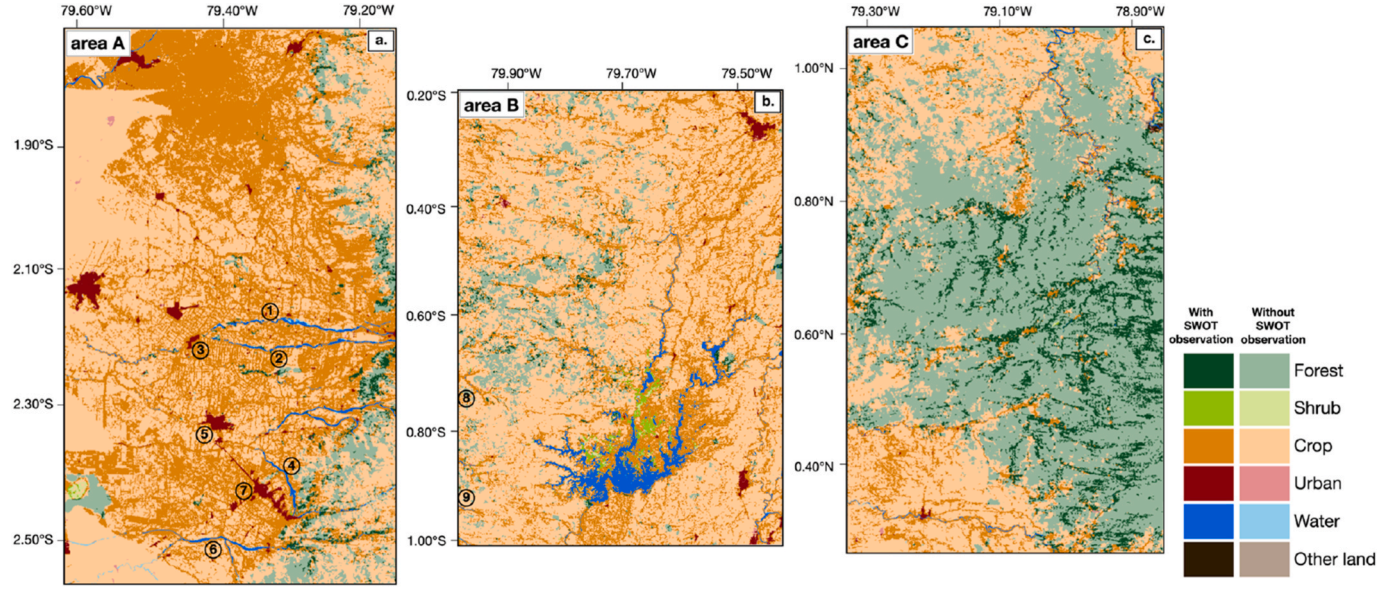

Fig. 5. Overlay of SWOT observations on the MAATE's 2022 reference LULC map, used for spatial validation. The darker shades (With SWOT) represent pixels from the Ministry's LULC map with SWOT observations, and the lighter shades (Without SWOT) indicate areas without SWOT observations for a) area A with 1. the Chimbo river, 2. the Chanchan river, 3. the city of Coronel Marcelino Maridueña, 4. the Bulubulu river, 5. the city of El Triunfo, 6. the Canar river and 7. the city of La Troncal b) area B with 8. downstream from La Esperanza dam and 9. downstream from the Multiproposito Chone dam c) area C.

3.2. Comparison of SWOT classification with ancillary datasets

To compare the cover type classification obtained from SWOT data with the LULC maps of the Ministry of the Environment, confusion matrices were computed for the three study areas considering only pixels where SWOT detections were recorded (Fig. 5). The absence of continuous SWOT data throughout the territory does not allow a systematic comparison with the reference maps of the Ministry of the Environment. To evaluate the performance of the classification obtained with the SVM, three metrics were calculated from the confusion matrices: Accuracy, F1-Score and Matthew Correlation Coefficient (MCC) for each of the three areas (Fig. 6). In general, for the three zones, Accuracy and F1-Score show high values. Accuracy varies between 0.87 for area A to more than 0.90 for areas B and C. The F1-Score varies between 0.89 for area A and 0.91 for areas B and C. These high values indicate with Accuracy, a good overall classification performance and with F1-score, a good ability of the model to correctly detect minority classes. However, differences are observed depending on the study areas for the MCC. Area B shows the best MCC of 0.63, reflecting a stable overall performance even in the presence of unbalanced classes. Area A, on the other hand, has the lowest MCC (0.34), which is explained by the fact that the Ministry of the Environment does not provide information on road that are widely detected by SWOT in this area. Thus, the roads not provided by the Ministry and classified as agricultural land have an impact on the MCC. Finally, area C achieves intermediate performances with an MCC of 0.44. The specificity of this area is the significant forest cover. More than 50% of SWOT detections are contained in the forest class of maps provided by the Ministry. These detections in the forest cover affect the MCC. These differences may be related to the fact that the Ministry of the Environment map used dates from 2022 and that the SWOT detections are analysed for the year 2024. These SWOT detections in the forest cover can indicate changes in LULC, but also human activities in the forest area.

These results confirm that the SWOT data, combining temporal and radiometric information, allows an automatic classification, but whose performance remains sensitive to the complexity of the local landscape and the quality of the reference data.

The comparison of the SWOT-based classification with CuSum detections and RADD Alerts in Area C shows that 39.6% and 40.7% of SWOT detections are contained in forest cover (Fig. 7). These detections may be related to human activity or environmental dynamics in wetlands under the forest cover that are not detected by radar. RADD and CuSum are based on Sentinel-1 data, which have a much higher angle of incidence than SWOT. Therefore, these methods may be more affected by topographic effects, especially in the southeastern part of study area C located in the Andean foothills. Additionally, Sentinel-1 operates in the C-band, which has limited penetration through vegetation, resulting in less sensitivity to subcanopy dynamics compared to the Ka-band used by SWOT.

4. Discussion

4.1. High resolution river streams mapping

The SWOT mission was initially designed to address major hydrological challenges, in particular the detection and characterization of rivers at least 100m wide (Biancamaria et al., 2016; JPL, 2024). In this context, our results confirm that SWOT allows a reliable detection of rivers on the studied areas. This ability to better represent the hydrographic network is an essential contribution to improving hydrological inventories and modeling river dynamics. For instance, at the center of study area A, the MAATE maps provide information on the Chimbo and Chanchan rivers at the level of the city of Coronel Marcelino Maridueña as well as the widest part of the Bulubulu river at the level of the city of El Triunfo (Fig. 5a). Between the two, no rivers are reported by the MAATE yet well marked on Open Street Map. Several other rivers are detected such as the Barranco Alto River or the Culebras By Pass 3 River which can reach a width of less than 30 m in some places. Further south of zone A, the Cochancay River is not listed by the MAATE but was detected by SWOT (Fig. 4a). To the southwest of Area B, the river that flow downstream from La Esperanza Dam is detected both by SWOT and by MAATE (Figs. 4b and 5b). However, further north, the Grande River downstream of the Multiproposito Chone dam is only detected by SWOT. Thus, SWOT could be a complementary dataset to the MAATE's LULC data by filling a data gap on river mapping. Our analyses confirm those of Normandin et al. (2024), which indicate that SWOT can detect streams much smaller than 100 m wide. In addition to the initial hydrological objectives, the SWOT data allowed to give hydrological information in complex ecosystems under a wet and dense forest cover and with significant topography. The southeast of zone C (Fig. 4c) is in the Andean piedmont and is characterized by significant slopes. This area has a dense forest cover and a humid tropical climate. In this complex environment, no image is visible on Google Earth. Optical images such as Sentinel-2 are unusable because they are largely affected by the persistent cloud cover throughout the entire study area. SWOT therefore makes it possible to provide observations on these areas where very few data are available and to bring new elements on the environmental dynamics in these regions. In this area, SWOT observations that were classified as no-forest by SVM and with low backscatter were analysed in relation to Apple images and the LULC map provided by GLAD. The

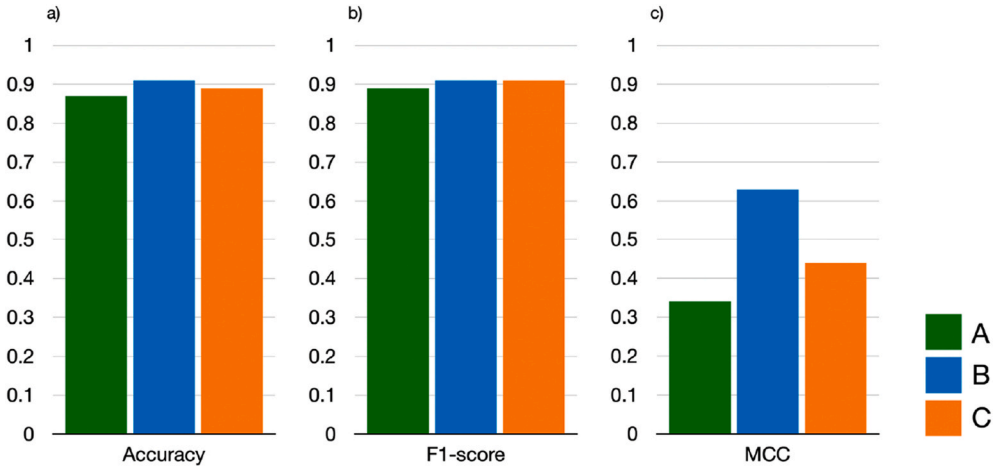

Fig. 6. Confusion matrix metrics resulting from the comparison between SWOT-based classification and MAATE LULC for area A (green), B (blue) and C (orange). a) Accuracy, b) F1-Score and c) MCC.

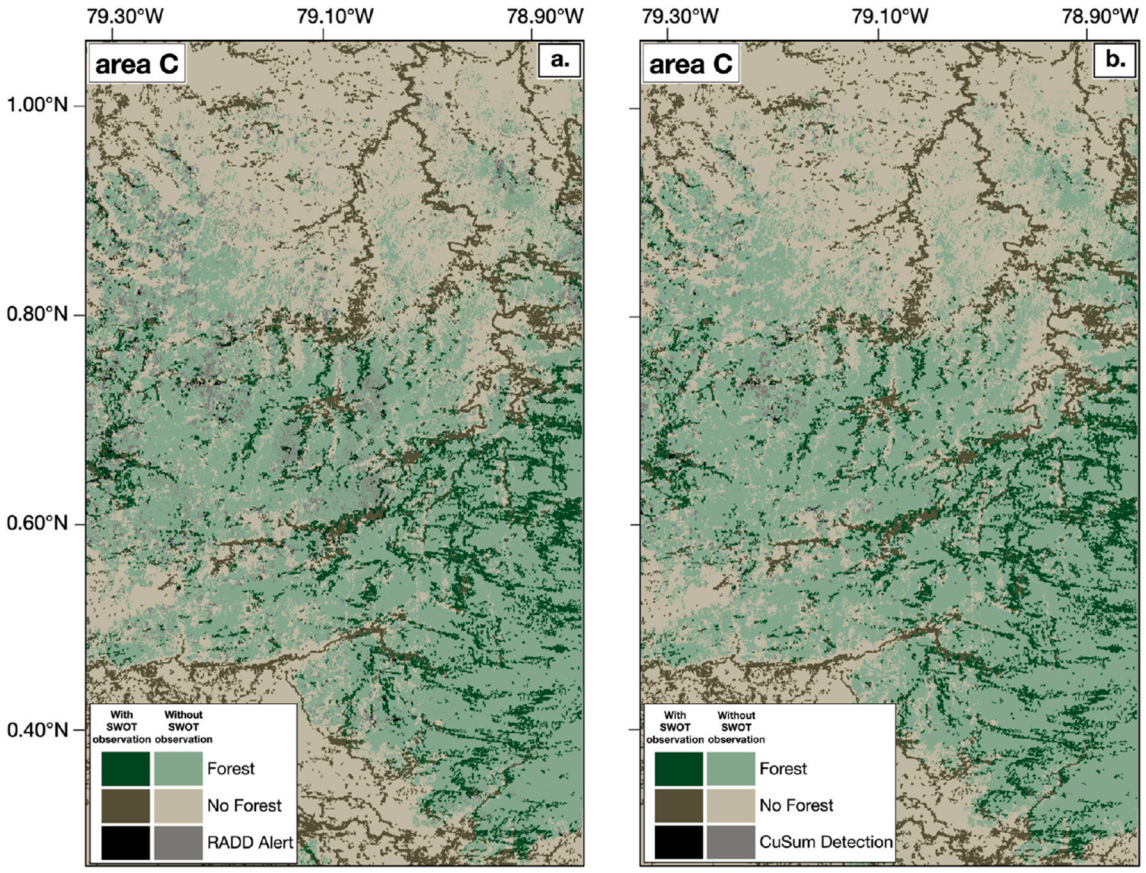

Fig. 7. Overlay of SWOT observations on a) the RADD detection map for the year 2024 and b) CuSum detection for the year 2024 for area C. The darker shades represent pixels from the RADD detection map or CuSum detections in areas with SWOT observations, and the lighter shades indicate areas without SWOT observations.

linear structures crossing the forest cover to the east of the zone correspond to streams that have not been properly classified by SVM (Fig. 4c). The classification of SWOT observations remains difficult in a complex environment largely affected by significant topography. Nevertheless, SWOT can provide information on small rivers and streams under the canopy (Fig. 8) that are not indicated on the GLAD map as in the west of zone 2 of Fig. 8. However, both products, GLAD and SWOT can be complementary. Both GLAD and SWOT fail to detect streams continuously. GLAD classifies certain segments as forests, and SWOT can identify these missing sections, for example in zones 1 and 2 of Fig. 8, highlighting the complementarity of the two products. The correct classification of these streams under forest cover remains difficult because the complex environment greatly affects radar backscatter. These rivers used as communication routes can pave the way for deforestation roads that SWOT can detect.

Other SWOT detections around rivers may indicate wetlands under forest cover. The Global Lakes and Wetlands Database (GLWD) (Lehner et al., 2025) classifies the entire study area C as forest peatland. SWOT detections could better locate these wetlands under the forest canopy. These ecosystems, among the largest carbon sinks on the planet (Page et al., 2011; Dargie et al., 2017), remain poorly known and undermapped. Up to now, radar altimetry was the only EO sensor able to continuously monitor wetlands under dense canopy cover but with low spatial coverage (Frappart et al., 2011, 2021a,b; Lee et al., 2015; Yuan et al., 2017). The information provided by SWOT could make it possible to better target their location, thus paving the way for further research on carbon storage, the resilience of these environments and the impacts of land use changes. For example, the detections around the Rio Agua Clara could correspond to a wetland under forest cover, as shown in zoom 3 (Fig. 8a). The Ministry of Agriculture reports in this area an Andisol soil type, which has a structure that can lead to exceptionally high water and nutrient retention capacity. SWOT therefore provides information in areas where other sources of information are limited. Optical imaging is constrained by persistent cloud cover throughout the year. Methods like CuSum or RADD do not detect any change due to the limitations of Sentinel-1 in terms of shadow effects and high incidence angle (Bouvet et al., 2018). SWOT, thanks to its low angle of incidence, manages to provide unprecedented information in these environments, even under dense forest cover. SWOT thus fills a lack of information in these areas difficult to access and where little information is available from remote sensing.

4.2. *Detailed information and complementary information for LULC*

In addition to the information that SWOT can provide regarding the hydrographic network and wetlands, SWOT can also provide information on areas of deforestation or forest cover degradation. Zone C is the only area where forest cover is dense and continuous. To the east of zone C, several SWOT observations are highlighted around river and indicate a degradation of forest cover, as shown in zoom 1(Fig. 9a) or deforestation, as shown in zoom 2 (Fig. 9a) visible in Apple images. Fig. 9 therefore illustrates the complementarity of SWOT observations and soil occupancy maps. Unlike GLAD, SWOT detects forest cover degradation and deforestation around these rivers or communication routes. For example, in zone 2 of Fig. 9, the SWOT observations correspond well to deforestation that is visible on the Apple image, while GLAD classify this area as a stable forest cover in a wetland area. Thus, all of the information provided by SWOT related to hydrography or forms of deforestation (deforestation route, forest cover degradation) in area C, explains the differences between SWOT observations and MAATE, RADD and

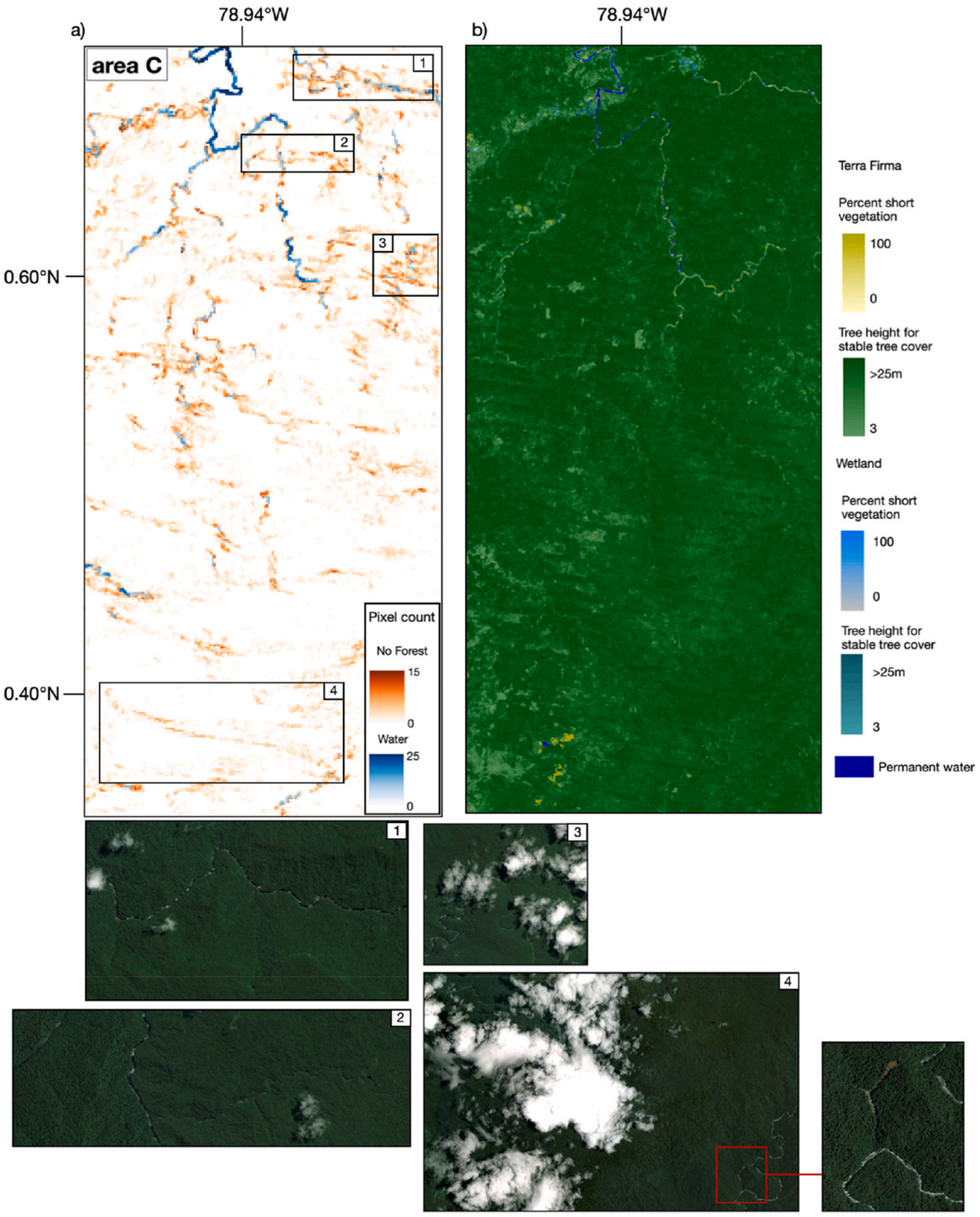

Fig. 8. a) Zoom on four zones of zone C. Zone 1 on the San Miguel river, Zone 2 and 3 on two zones of the Agua Clara river, and zone 4 on the Canande river in the northwest of the zone and the Naranjal river in the southeast. All the satellite images used to illustrate the SWOT observations are distributed by Apple. b) GLAD's LULC map for the year 2020. This product from GLAD provides the percentage of short vegetation as well as the tree height of the forest cover on land (terra firma) and on wetlands. Both GLAD and SWOT fail to provide continuous river detection. GLAD classifies certain river segments as stable tree cover, while SWOT can identify and characterize these missing sections.

CuSum maps. SWOT allows detecting environmental dynamics under forest cover and human activities in complex environments, which explains why pixels are classified as water or no-forest in areas classified as Forest by MAATE, RADD or CuSum.

SWOT also provides relevant information on agricultural practices. In area A, the SWOT observations allow to see the fine delimitation of the plots. These observations can be paralleled with the map of the Ecuadorian Ministry of Agriculture which provides information on crop types (Fig. 10). The agricultural plot boundaries obtained with SWOT data at the center of area A, correspond to the boundaries of the plots for sugar cane crops provided by the Ministry of Agriculture. SWOT can therefore provide spatial information on agricultural occupation and be a source of complementary information in other regions that have little data on agricultural plots. In addition, in areas A and B, SWOT has the ability to provide information on the type of crop present and the state of field flooding. The results of the number of SWOT occurrences showed

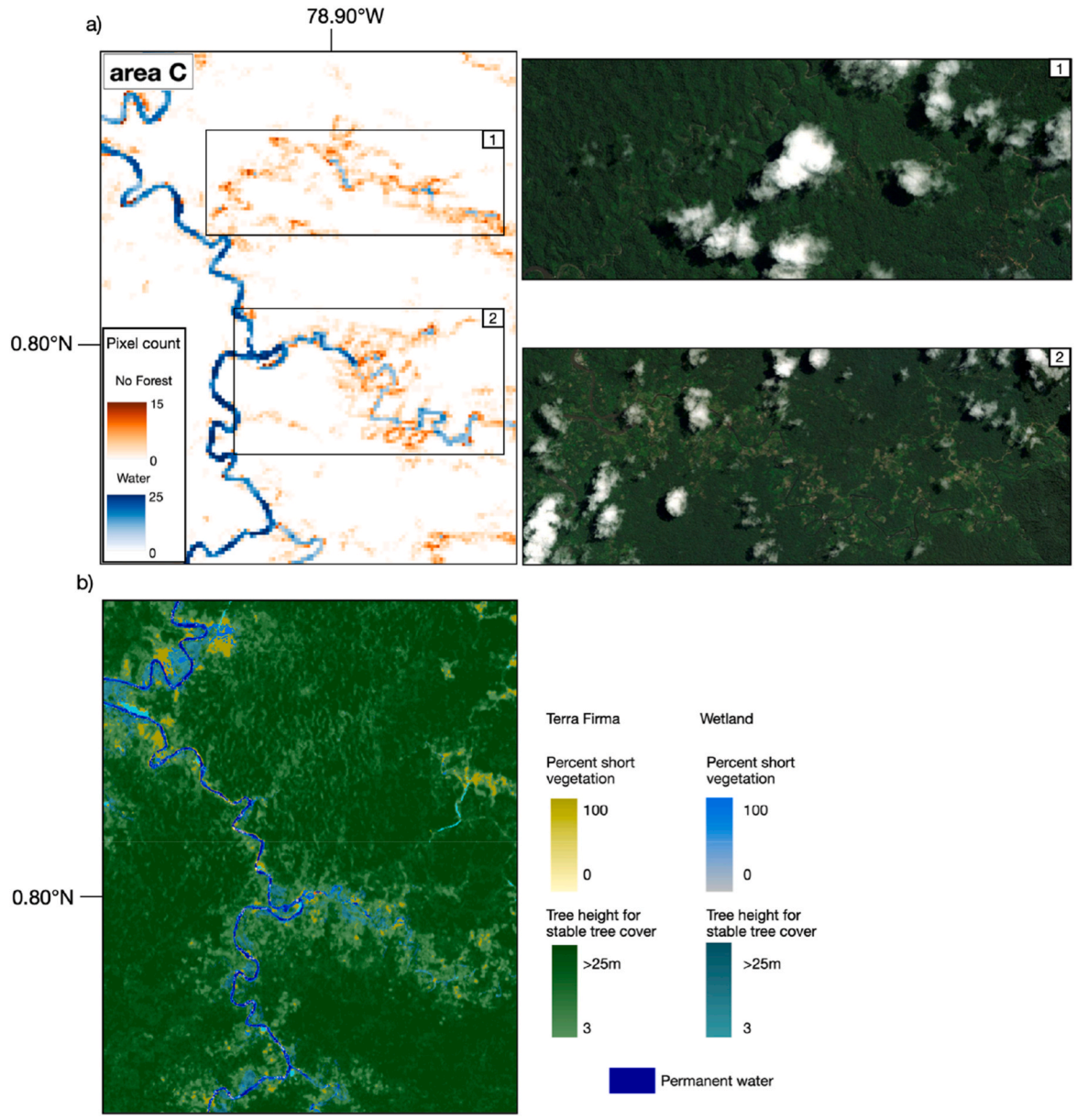

Fig. 9. a) Zoom on two zones in area C. Zone 1 is located on the Zapotillo river and corresponds to a forest cover degradation area. Zone 2 on the Zapallo river and corresponds to a deforestation area. b) GLAD's LULC map for the year 2020 indicates a stable tree cover in terra firma for zone 1 and a stable tree cover in wetland for zone 2.

that agricultural areas provide very heterogeneous values, particularly in area A. These spatial variations are partly related to the type of agriculture and the use of irrigation (Fig. 10). Mainly located in the north of zone A, the data from the Ministry of Agriculture provide information on three cycles of rice cultivation. The average value of monthly sig0 was calculated based on these three crop cycles (Fig. 11). Fig. 10 provides information on the plots used for cycle 1, 2, and 3 of rice cultivation for the year 2024. The Ministry informs the dates of sowing for each cycle. For the first cycle, sowing was completed between December 2023 and March 2024 (Leiva et al., 2025). For the second cycle, sowing was carried out between April and June 2024 (León et al., 2025). For the third cycle, sowing was carried out between August and September 2024 (Muyulema et al., 2025). The variations in sig0 obtained with SWOT data correspond to the periods of sowing, growth, and rice cultivation. The obtained variations also agree with the precipitation data observed in the Guyas basin. The months from January to April correspond to the rainy season, which explains the high values of the Sig0 during this period. The following months correspond to the dry season, which explains the lower Sig0 values (Frappart et al., 2017). Thus, SWOT data can allow the monitoring of agricultural practices. Even if the limited SWOT coverage does not allow this analysis to be carried out on all crop types, SWOT data opens perspectives for monitoring agricultural productivity. Similarly, Bazzi et al., (2026a,b) have already demonstrated the capacity of SWOT to monitor irrigation on irrigated plots.

The results also suggest that some road axes can be identified using SWOT data. Although this application is not part of the initial objectives of the mission, it offers an opportunity to monitor infrastructure expansion. Mapping of roads is key as roads are a determining factor in the transformation of landscapes, particularly in connection with deforestation and agricultural expansion (Laurance et al., 2014).

Despite these contributions, SWOT does not allow an exhaustive classification over the entire study area. Its products must therefore be considered as complementary to existing databases, such as the maps of

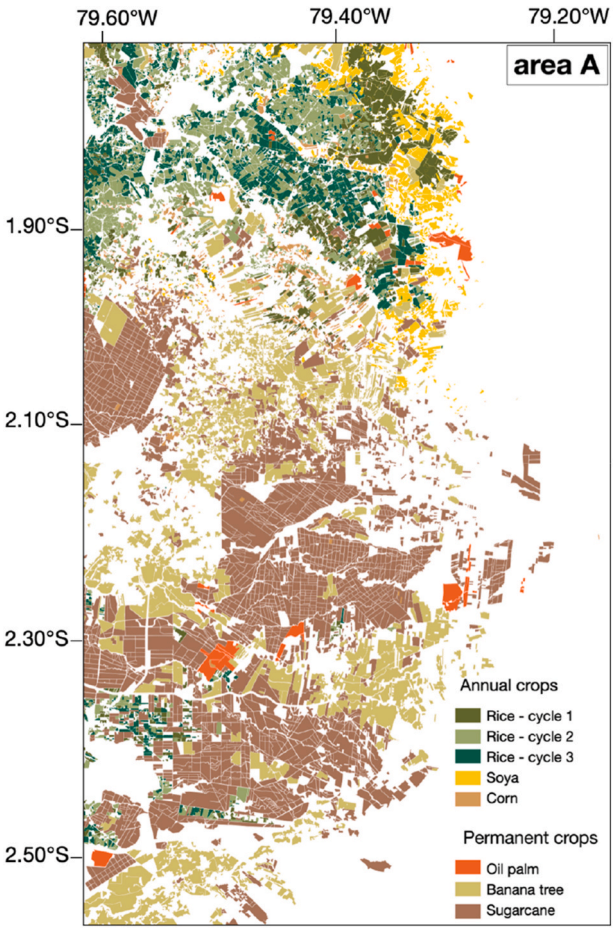

Fig. 10. Type of annual and permanent crops provided by the Ecuadorian Ministry of Agriculture in area A for the year 2024.

the Ministry of Agriculture, but they have the advantage of informing areas hitherto very little documented, such as dense forests located in rugged regions. Finally, a dispersion of data is observed around the detection of rivers, especially in areas of steep slopes. This phenomenon, already reported in the literature (Normandin et al., 2024), reflects the sensitivity of SWOT measurements to topographic constraints. Correction methods will need to be developed to limit this bias and improve the accuracy of derivatives.

5. Conclusion

If SWOT was initially designed for applications in hydrology and oceanography, its advanced technology opens the way to new applications. This research explored an innovative use of SWOT to analyse land cover in three areas of the Pacific Coast of Ecuador. The study aimed to evaluate the potential of SWOT analysis to supplement existing land use and land cover (LULC) products. To study land use from SWOT data, we used the available sig0 from the SWOT raster product at 100m resolution for the year 2024. Two maps were obtained: the number of pixel occurrences, providing the observation frequency per pixel, and the average of the sig0, representing the average intensity of the backscattered signal. These two maps provided spatial and temporal information that allowed to highlight spatial patterns in order to characterize land use and discriminate between the main classes of soil occupation. These two maps were subsequently used to train a machine learning model. The SVM used was trained on four classes (city, water, road and crop or No Forest) to obtain a classification of land use over the three study areas. The SWOT-based automatic classification allowed to classify the four classes for zone A and C, but not for the very few roads present in area B. All these observations were compared with the soil occupancy maps of the Ecuadorian Ministry of the Environment and with two products of detected changes in forest cover for Area C. These comparisons made it clear that SWOT allows providing additional information compared to existing products. For instance, in the three study areas, the SWOT detections made it possible to highlight watercourses that can reach 30m in width which are not indicated in the maps of the Ministry of the environment. In addition to improving the mapping of watercourses, SWOT can provide detailed information on land occupation. SWOT detections highlighted the road axes and the boundaries of agricultural plots in zone A, as well as deforestation routes in zone C. The SWOT data also allowed for the detection of recent forms of deforestation in the north of the study area. Thus, SWOT can fill a lack of information in regions with significant topography and densely vegetated regions thanks to its low angle of incidence. In these areas, optical observations are limited by frequent clouds and radar data, such as Sentinel 1, due to their sensitivity to topographic effects. SWOT can also provide information on agricultural practices for use in crop

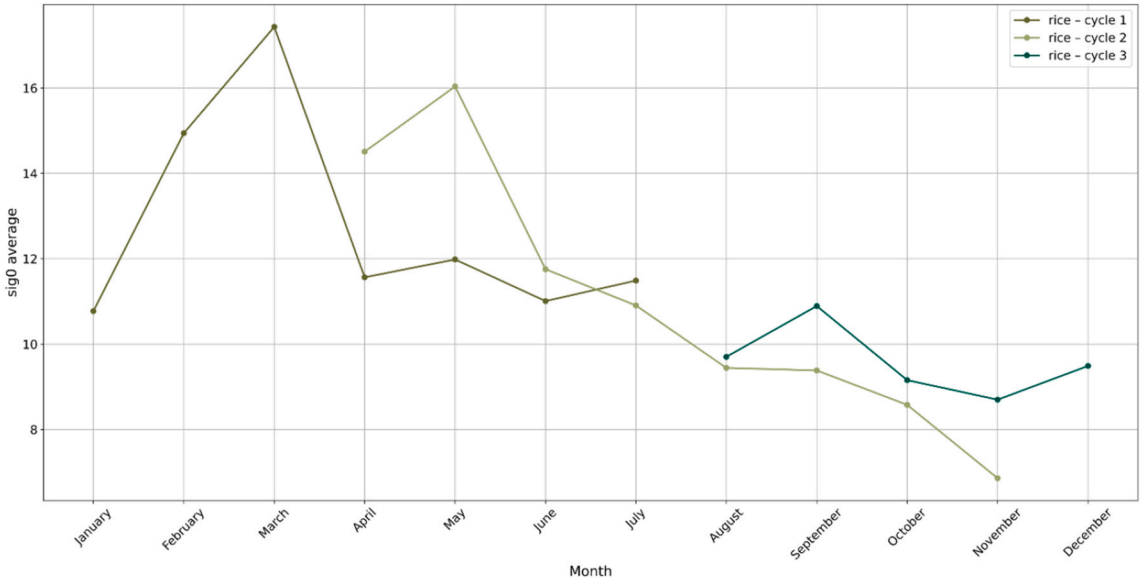

Fig. 11. Monthly average SWOT sig0 based on the three rice growing cycles in area A for the year 2024.

monitoring in areas where SWOT data are available.

The exploratory results obtained in this study demonstrated the feasibility and potential of using SWOT data to monitor changes in Land Use and Land Cover (LULC). Future work will involve exploiting longer SWOT time series covering the period from 2024 to 2026, in order to assess land cover change dynamics. Future work will also analyse Single Look Complex (SLC) products, which offer more continuous spatial coverage than the raster products used in the present study and constitute a promising perspective.

CRediT authorship contribution statement

Valentine Sollier: Writing – review & editing, Writing – original draft, Visualization, Validation, Supervision, Software, Resources, Project administration, Methodology, Investigation, Funding acquisition, Formal analysis, Data curation, Conceptualization. **Frédéric Frappart:** Writing – review & editing, Supervision, Project administration, Methodology, Investigation, Funding acquisition, Conceptualization. **Luc Bourrel:** Writing – review & editing, Supervision, Project administration, Methodology, Investigation, Funding acquisition, Conceptualization. **Bertrand Ygorra:** Writing – review & editing, Supervision, Project administration, Methodology, Investigation, Funding acquisition, Data curation, Conceptualization. **Cassandra Normandin:** Writing – review & editing, Supervision, Project administration, Methodology, Investigation, Funding acquisition, Conceptualization. **Luis Huaraca:** Writing – review & editing, Project administration, Investigation, Funding acquisition, Data curation. **ThomasL.P. Couvreur:** Writing – review & editing. **Edward Salameh:** Writing – review & editing. **Nicolas Baghdadi:** Writing – review & editing, Supervision. **Jean-Pierre Wigneron:** Writing – review & editing, Supervision.

Funding

This study was supported by the MELICERTES project (ANR-22-PEAE-0010) of the French National Research Agency, under the France2030 program and the national PEPR “agroécologie et numérique” program. This study was also supported by the PNTS N°PNTS-2023-11-TestReTroForRS.

Declaration of competing interest

The authors declare that they have no known competing financial interests or personal relationships that could have appeared to influence the work reported in this paper.

Data availability

The data is freely accessible.

References

Armenteras, D., Espelta, J.M., Rodríguez, N., Retana, J., 2017. Deforestation dynamics and drivers in different forest types in Latin America: three decades of studies (1980–2010). Glob. Environ. Change 46, 139–147. https://doi.org/10.1016/j.gloenvcha.2017.09.002.

Barlow, J., Lennox, G.D., Ferreira, J., Berenguer, E., Lees, A.C., Nally, R.M., Thomson, J. R., Ferraz, S.F. de B., Louzada, J., Oliveira, V.H.F., Parry, L., Ribeiro de Castro Solar, R., Vieira, I.C.G., Aragão, L.E.O.C., Begotti, R.A., Braga, R.F., Cardoso, T.M., de Oliveira, R.C., Souza Jr, C.M., Moura, N.G., Nunes, S.S., Siqueira, J.V., Pardini, R., Silveira, J.M., Vaz-de-Mello, F.Z., Veiga, R.C.S., Venturieri, A., Gardner, T.A., 2016. Anthropogenic disturbance in tropical forests can double biodiversity loss from deforestation. Nature 535, 144–147. https://doi.org/10.1038/nature18326.

Bazzi, H., Baghdadi, N., Cazals, C., Maleki, S., Zribi, M., Frappart, F., 2026a. Temporal behavior of major crops with SWOT Ka-band SAR observations. GIScience & Remote Sensing 63, 2620174. https://doi.org/10.1080/15481603.2026.2620174.

Bazzi, H., Baghdadi, N., Cazals, C., Najem, S., Desroches, D., Frappart, F., Zribi, M., Charron, F., 2026b. Observing irrigation using SWOT SAR Ka-band data from daily calibration and validation acquisitions. Science of Remote Sensing 13, 100378. https://doi.org/10.1016/j.srs.2026.100378.

Biancamaria, S., Lettenmaier, D.P., Pavelsky, T.M., 2016. The SWOT Mission and Its Capabilities for Land Hydrology. Surv Geophys 37, 307–337. https://doi.org/10.1007/s10712-015-9346-y.

Bossy, T., Ciais, P., Renaudineau, S., Wan, L., Ygorra, B., Adam, E., Barbier, N., Bauters, M., Delbart, N., Frappart, F., Gara, T.W., Hamunyela, E., Ifo, S.A., Jaffrain, G., Maisongrande, P., Mugabowindekwe, M., Mugiraneza, T., Normandin, C., Obame, C.V., Peaucelle, M., Pinet, C., Ploton, P., Sagang, L.B., Schwartz, M., Sollier, V., Sonké, B., Tresson, P., De Truchis, A., Vo Quang, A., Wigneron, J.-P., 2025. State of the art in remote sensing monitoring of carbon dynamics in African tropical forests. Front. Remote Sens. 6, 1532280. https://doi.org/10.3389/frsen.2025.1532280.

Bouvet, A., Mermoz, S., Ballère, M., Koleck, T., Le Toan, T., 2018. Use of the SAR Shadowing Effect for Deforestation Detection with Sentinel-1 Time Series. Remote Sensing 10, 1250. https://doi.org/10.3390/rs10081250.

Brown, C.F., Brumby, S.P., Guzder-Williams, B., Birch, T., Hyde, S.B., Mazzariello, J., Czerwinski, W., Pasquarella, V.J., Haertel, R., Ilyushchenko, S., Schwehr, K., Weisse, M., Stolle, F., Hanson, C., Guinan, O., Moore, R., Tait, A.M., 2022. Dynamic world, near real-time global 10 m land use land cover mapping. Sci. Data 9, 251. https://doi.org/10.1038/s41597-022-01307-4.

Chicco, D., Jurman, G., 2020. The advantages of the matthews correlation coefficient (MCC) over F1 score and accuracy in binary classification evaluation. BMC Genom. 21, 6. https://doi.org/10.1186/s12864-019-6413-7.

Copernicus Climate Change Service, 2019. Land cover classification gridded maps from 1992 to present derived from satellite observations. https://doi.org/10.24381/CDS.006F2C9A.

Cretaux, J.-F., Calmant, S., Papa, F., Frappart, F., Paris, A., Berge-Nguyen, M., 2023. Inland Surface Waters Quantity Monitored from Remote Sensing. Surv Geophys 44, 1519–1552. https://doi.org/10.1007/s10712-023-09803-x.

Daily, G.C. (Ed.), 1997. Nature's Services: Societal Dependence on Natural Ecosystems. Island Press, Washington, DC.

Dargie, G.C., Lewis, S.L., Lawson, I.T., Mitchard, E.T.A., Page, S.E., Bocko, Y.E., Ifo, S.A., 2017. Age, extent and carbon storage of the central Congo Basin peatland complex. Nature 542, 86–90. https://doi.org/10.1038/nature21048.

FAO, 2022. FRA 2020 Remote Sensing Survey, FAO Forestry Paper. FAO, Rome. https://doi.org/10.4060/cb9970en.

Fayne, J.V., Smith, L.C., Liao, T.-H., Pitcher, L.H., Denbina, M., Chen, A.C., Simard, M., Chen, C.W., Williams, B.A., 2024. Characterizing near-nadir and low incidence Ka-Band SAR backscatter from wet surfaces and diverse land covers. IEEE J. Sel. Top. Appl. Earth Obs. Rem. Sens. 17, 985–1006. https://doi.org/10.1109/JSTARS.2023.3317502.

Fjortoft, R., Gaudin, J.-M., Pourthie, N., Lalaurie, J.-C., Mallet, A., Nouvel, J.-F., Martinot-Lagarde, J., Oriot, H., Borderies, P., Ruiz, C., Daniel, S., 2014. KaRIn on SWOT: characteristics of near-nadir Ka-Band interferometric SAR imagery. IEEE Trans. Geosci. Rem. Sens. 52, 2172–2185. https://doi.org/10.1109/TGRS.2013.2258402.

Foley, J.A., DeFries, R., Asner, G.P., Barford, C., Bonan, G., Carpenter, S.R., Chapin, F.S., Coe, M.T., Daily, G.C., Gibbs, H.K., Helkowski, J.H., Holloway, T., Howard, E.A., Kucharik, C.J., Monfreda, C., Patz, J.A., Prentice, I.C., Ramankutty, N., Snyder, P.K., 2005. Global consequences of land use. Science 309, 570–574. https://doi.org/10.1126/science.1111772.

França, F.M., Benkwitt, C.E., Peralta, G., Robinson, J.P.W., Graham, N.A.J., Tylianakis, J. M., Berenguer, E., Lees, A.C., Ferreira, J., Louzada, J., Barlow, J., 2020. Climatic and local stressor interactions threaten tropical forests and coral reefs. Philos. Trans. R. Soc. B 375, 20190116. https://doi.org/10.1098/rstb.2019.0116.

Frappart, F., Papa, F., Güntner, A., Werth, S., Santos Da Silva, J., Tomasella, J., Seyler, F., Prigent, C., Rossow, W.B., Calmant, S., Bonnet, M.-P., 2011. Satellite-based estimates of groundwater storage variations in large drainage basins with extensive floodplains. Rem. Sens. Environ. 115, 1588–1594. https://doi.org/10.1016/j.rse.2011.02.003.

Frappart, F., Fatras, C., Mougin, E., Marieu, V., Diepkilé, A.T., Blarel, F., Borderies, P., 2015. Radar altimetry backscattering signatures at Ka, Ku, C, and S bands over West Africa. Phys. Chem. Earth, Parts A/B/C 83 (84), 96–110. https://doi.org/10.1016/j.pce.2015.05.001.

Frappart, F., Bourrel, L., Brodu, N., Riofrío Salazar, X., Baup, F., Darrozes, J., Pombosa, R., 2017. Monitoring of the spatio-temporal dynamics of the floods in the Guayas watershed (ecuadorian Pacific Coast) using global monitoring ENVISAT ASAR images and rainfall data. Water 9, 12. https://doi.org/10.3390/w9010012.

Frappart, F., Blarel, F., Papa, F., Prigent, C., Mougin, E., Paillou, P., Baup, F., Zeiger, P., Salameh, E., Darrozes, J., Bourrel, L., Rémy, F., 2021a. Backscattering signatures at Ka, Ku, C and S bands from low resolution radar altimetry over land. Adv. Space Res. 68, 989–1012. https://doi.org/10.1016/j.asr.2020.06.043.

Frappart, F., Zeiger, P., Betbeder, J., Gond, V., Bellot, R., Baghdadi, N., Blarel, F., Darrozes, J., Bourrel, L., Seyler, F., 2021b. Automatic detection of inland water bodies along altimetry tracks for estimating surface water storage variations in the Congo Basin. Remote Sens. 13, 3804. https://doi.org/10.3390/rs13193804.

Friedl, M., Sulla-Menashe, D., 2019. MCD12Q1 MODIS/terra+Aqua land cover type yearly L3 global 500m SIN grid V006. https://doi.org/10.5067/MODIS/MCD12Q1.006.

Fu, L., Pavelsky, T., Cretaux, J., Morrow, R., Farrar, J.T., Vaze, P., Sengenes, P., Vinogradova-Shiffer, N., Sylvestre-Baron, A., Picot, N., Dibarboure, G., 2024. The surface water and ocean topography mission: a breakthrough in radar remote sensing of the ocean and land surface water. Geophys. Res. Lett. 51. https://doi.org/10.1029/2023GL107652 e2023GL107652.

Hansen, M.C., Potapov, P.V., Moore, R., Hancher, M., Turubanova, S.A., Tyukavina, A., Thau, D., Stehman, S.V., Goetz, S.J., Loveland, T.R., Kommareddy, A., Egorov, A., Chini, L., Justice, C.O., Townshend, J.R.G., 2013. High-resolution global maps of

21st-Century forest cover change. Science 342, 850–853. https://doi.org/10.1126/science.1244693.
IPBES, 2019. Summary for Policymakers of the Global Assessment Report on Biodiversity and Ecosystem Services of the Intergovernmental Science-Policy Platform on Biodiversity and Ecosystem Services. IPBES.
JPL, D-105507, 2024. SWOT Algorithm Theoretical Basis Document: Level 2 KaRIn High Rate Raster (L2_HR_Raster) Science Algorithm Software. Jet Propulsion Laboratory Internal Document.
JPL, D-56416, Revision, C, 2025. SWOT Product Description Document: Level 2 KaRIn High Rate Raster (L2_HR_Raster) Data Product. Jet Propulsion Laboratory Internal Document.
Kica, S., Pavelsky, T.M., Fayne, J.V., Williams, B.A., 2025. SWOT water surface elevation in herbaceous wetlands of florida's everglades. Geophys. Res. Lett. 52. https://doi.org/10.1029/2025GL114956 e2025GL114956.
Krieger, D., 2001. Economic value of forest ecosystem services: a review. The Wilderness Society 1615.
Laurance, W.F., Sayer, J., Cassman, K.G., 2014. Agricultural expansion and its impacts on tropical nature. Trends Ecol. Evol. 29, 107–116. https://doi.org/10.1016/j.tree.2013.12.001.
Lee, H., Yuan, T., Jung, H.C., Beighley, E., 2015. Mapping wetland water depths over the central Congo Basin using PALSAR ScanSAR, envisat altimetry, and MODIS VCF data. Rem. Sens. Environ. 159, 70–79. https://doi.org/10.1016/j.rse.2014.11.030.
Lehner, B., Anand, M., Fluet-Chouinard, E., Tan, F., Aires, F., Allen, G.H., Bousquet, P., Canadell, J.G., Davidson, N., Ding, M., Finlayson, C.M., Gumbricht, T., Hilarides, L., Hugelius, G., Jackson, R.B., Korver, M.C., Liu, L., McIntyre, P.B., Nagy, S., Olefeldt, D., Pavelsky, T.M., Pekel, J.-F., Poulter, B., Prigent, C., Wang, J., Worthington, T.A., Yamazaki, D., Zhang, X., Thieme, M., 2025. Mapping the world's inland surface waters: an upgrade to the global Lakes and wetlands database (GLWD v2). Earth Syst. Sci. Data 17, 2277–2329. https://doi.org/10.5194/essd-17-2277-2025.
Leiva, D., León, D., Simbaña, B., Villarreal, W., Yépez, R., 2025. Estimación de superficie sembrada del cultivo de arroz (oryza sativa l.) del primer período (época lluviosa) año 2024, en las provincias de guayas, los ríos, manabí, loja, el oro y cañar. Coordinación General de Información Nacional Agropecuaria - Dirección de Generación de Geoinformación Agropecuaria, Quito - Ecuador.
León, D., Rodríguez, A., Romero, E., Vasquez, D., Villarreal, W., Yépez, R., 2025. Estimación de superficie sembrada del cultivo de arroz (oryza sativa l.) del segundo período (época seca) año 2024, en las provincias de guayas, los ríos, manabí, loja, el oro y cañar. Coordinación General de Información Nacional Agropecuaria - Dirección de Generación de Geoinformación Agropecuaria, Quito - Ecuador.
Matthews, R.B., Van Noordwijk, M., Lambin, E., Meyfroidt, P., Gupta, J., Verchot, L., Hergoualc'h, K., Veldkamp, E., 2014. Implementing REDD+ (reducing emissions from deforestation and degradation): evidence on governance, evaluation and impacts from the REDD-ALERT project. Mitig. Adapt. Strategies Glob. Change 19, 907–925. https://doi.org/10.1007/s11027-014-9578-z.
Ministerio del Ambiente, 2017. Deforestación Del Ecuador Continental Periodo 2014-2016. Quito-Ecuador.
Mosandl, R., Günter, S., Stimm, B., Weber, M., 2008. Ecuador suffers the highest deforestation rate in South America. In: Beck, E., Bendix, J., Kottke, I., Makeschin, F., Mosandl, Reinhard (Eds.), Gradients in a Tropical Mountain Ecosystem of Ecuador, Ecological Studies. Springer, Berlin Heidelberg, Berlin, Heidelberg, pp. 37–40. https://doi.org/10.1007/978-3-540-73526-7_4.
Muyulema, W., Rodríguez, A., Romero, E., Vásquez, D., Yépez, R., 2025. Estimación de superficie sembrada del cultivo de arroz (oryza sativa l.) del tercer período (época seca) año 2024, en las provincias de guayas y los ríos. Coordinación General de Información Nacional Agropecuaria - Dirección de Generación de Geoinformación Agropecuaria, Quito - Ecuador.
Myers, N., 1988. Threatened biotas: "hot spots" in tropical forests. Environmentalist 8, 187–208. https://doi.org/10.1007/BF02240252.
Normandin, C., Frappart, F., Baghdadi, N., Bourrel, L., Peña Luque, S., Ygorra, B., Kitambo, B., Papa, F., Riazanoff, S., Wigneron, J.-P., 2024. First results of the surface water ocean topography (SWOT) observations to rivers elevation profiles in the Cuvette Centrale of the Congo Basin. Front. Remote Sens. 5, 1466695. https://doi.org/10.3389/frsen.2024.1466695.
Page, S.E., Rieley, J.O., Banks, C.J., 2011. Global and regional importance of the tropical peatland carbon pool. Glob. Change Biol. 17, 798–818. https://doi.org/10.1111/j.1365-2486.2010.02279.x.
Papa, F., Legrésy, B., Rémy, F., 2003. Use of the Topex–Poseidon dual-frequency radar altimeter over land surfaces. Rem. Sens. Environ. 87, 136–147. https://doi.org/10.1016/S0034-4257(03)00136-6.
Potapov, P., Hansen, M.C., Pickens, A., Hernandez-Serna, A., Tyukavina, A., Turubanova, S., Zalles, V., Li, X., Khan, A., Stolle, F., Harris, N., Song, X.-P., Baggett, A., Kommareddy, I., Kommareddy, A., 2022. The global 2000-2020 land cover and land use change dataset derived from the landsat archive: first results. Front. Remote Sens. 3. https://doi.org/10.3389/frsen.2022.856903.
Reiche, J., Mullissa, A., Slagter, B., Gou, Y., Tsendbazar, N.-E., Odongo-Braun, C., Vollrath, A., Weisse, M.J., Stolle, F., Pickens, A., Donchyts, G., Clinton, N., Gorelick, N., Herold, M., 2021. Forest disturbance alerts for the Congo Basin using Sentinel-1. Environ. Res. Lett. 16, 024005. https://doi.org/10.1088/1748-9326/abd0a8.
Renaudineau, S., Frappart, F., Peaucelle, M., Sollier, V., Wigneron, J.-P., Ciais, P., Ygorra, B., 2025. Forest cover in the Congo Basin: consistency evaluation of seven datasets. Forests 16, 1609. https://doi.org/10.3390/f16101609.
Rogan, J., Chen, D., 2004. Remote sensing technology for mapping and monitoring land-cover and land-use change. Prog. Plann. 61, 301–325. https://doi.org/10.1016/S0305-9006(03)00066-7.
Salameh, E., Desroches, D., Deloffre, J., Fjørtoft, R., Mendoza, E.T., Turki, I., Froideval, L., Levaillant, R., Déchamps, S., Picot, N., Laignel, B., Frappart, F., 2024. Evaluating SWOT's interferometric capabilities for mapping intertidal topography. Rem. Sens. Environ. 314, 114401. https://doi.org/10.1016/j.rse.2024.114401.
Shimada, M., Itoh, T., Motooka, T., Watanabe, M., Shiraishi, T., Thapa, R., Lucas, R., 2014. New global forest/non-forest maps from ALOS PALSAR data (2007–2010). Rem. Sens. Environ. 155, 13–31. https://doi.org/10.1016/j.rse.2014.04.014.
Sollier, V., Frappart, F., Bourrel, L., Couvreur, T.L.P., Peaucelle, M., Renaudineau, S., Huaraca, L., Wigneron, J.-P., 2025. Long-term evolution of forest cover in the Pacific coast of Ecuador (1960–2019): a comparison of Land Use/Land Cover (LULC) remote sensing products. Front. Remote Sens. 6, 1536105. https://doi.org/10.3389/frsen.2025.1536105.
Turubanova, S., Potapov, P.V., Tyukavina, A., Hansen, M.C., 2018. Ongoing primary forest loss in Brazil, democratic Republic of the Congo, and Indonesia. Environ. Res. Lett. 13, 074028. https://doi.org/10.1088/1748-9326/aacd1c.
Vancutsem, C., Achard, F., Pekel, J.-F., Vieilledent, G., Carboni, S., Simonetti, D., Gallego, J., Aragão, L.E.O.C., Nasi, R., 2021. Long-term (1990–2019) monitoring of forest cover changes in the humid tropics. Sci. Adv. 7, eabe1603. https://doi.org/10.1126/sciadv.abe1603.
Vapnik, V.N., 1997. The support vector method. In: Gerstner, W., Germond, A., Hasler, M., Nicoud, J.-D. (Eds.), Artificial Neural Networks — ICANN'97, Lecture Notes in Computer Science. Springer, Berlin Heidelberg, Berlin, Heidelberg, pp. 261–271. https://doi.org/10.1007/BFb0020166.
Ygorra, B., Frappart, F., Wigneron, J.P., Moisy, C., Catry, T., Baup, F., Hamunyela, E., Riazanoff, S., 2021. Monitoring loss of tropical forest cover from Sentinel-1 time-series: a CuSum-based approach. Int. J. Appl. Earth Obs. Geoinf. 103, 102532. https://doi.org/10.1016/j.jag.2021.102532.
Yuan, T., Lee, H., Jung, H.C., Aierken, A., Beighley, E., Alsdorf, D.E., Tshimanga, R.M., Kim, D., 2017. Absolute water storages in the congo river floodplains from integration of InSAR and satellite radar altimetry. Rem. Sens. Environ. 201, 57–72. https://doi.org/10.1016/j.rse.2017.09.003.
Zanaga, D., Van De Kerchove, R., De Keersmaecker, W., Souverijns, N., Brockmann, C., Quast, R., Wevers, J., Grosu, A., Paccini, A., Vergnaud, S., Cartus, O., Santoro, M., Fritz, S., Georgieva, I., Lesiv, M., Carter, S., Herold, M., Li, L., Tsendbazar, N.-E., Ramoino, F., Arino, O., 2021. ESA WorldCover 10 m 2020 v100. https://doi.org/10.5281/ZENODO.5571936.